

# Prediction of the Internal Pressure Capacity at Liner Failure of the Small-scaled Prestressed Concrete Containment Vessel under Hydrogen Burning Conditions

Woo-Min Cho<sup>a</sup>, Seong-Kug Ha<sup>a</sup>, Han-Sang Woo<sup>b</sup>, Yoon-Suk Chang<sup>b\*</sup>

<sup>a</sup>Korea Institute of Nuclear Safety (KINS), 62 Gwahak-ro, Yuseong-gu, Daejeon 34142, Korea

<sup>b</sup>Kyung Hee University, 1732 Deogyong-daero, Giheung-gu, Yongin-si, Gyeonggi-do 17104, Korea

\*Corresponding author: yschang@khu.ac.kr

\***Keywords** : Internal Pressure Capacity, Liner Failure, Prestressed Concrete Containment Vessel, Hydrogen Burning

## 1. Introduction

Since the containment building is one of the most important shielding barriers for the nuclear reactor, its integrity should be ensured for nuclear safety. The major object of the containment building attached to the liner is to prevent releases of radioactive materials into the environment. Thus, the mechanical behavior and the internal pressure capacity of the containment building have been thoroughly studied. For the last 30 years, a lot of tests and numerical analyses of the small-scaled containment buildings subjected to internal pressure have been investigated [1]. Experimental studies have presented the failure modes and mechanical behaviors, such as the cracking or crushing of the concrete and the yielding of the steel [2,3]. Numerical studies have made up for the limitations of the tests due to their time and cost [2,3].

The preceding researches reported the potential vulnerability of the containment buildings under ultimate pressure conditions. However, the prediction of the internal pressure capacity of its structure under severe accident conditions has been overlooked due to its extremely low probability of outbreak, in spite of the subsequent serious situation [4]. For this reason, this paper focuses on the evaluation of the failure and performance by analyzing the thermal and mechanical behaviors of the containment building under hydrogen burning conditions at a station blackout.

## 2. Numerical Analysis of 1/4-scaled PCCV

### 2.1 Material Constitutive Models

To accurately capture the nonlinear and inelastic behavior of the prestressed concrete containment vessel (PCCV) components, the concrete damaged plasticity (CDP) model was adopted to account for concrete behavior under stress [5]. The compression and tension of the concrete were represented by the theoretical models suggested by Hognestad and Izumo, as described in Eqs. 1 and 2 [6,7].

$$\sigma_c = \begin{cases} f_c \left[ 2 \left( \frac{\varepsilon}{\varepsilon_0} \right) - \left( \frac{\varepsilon}{\varepsilon_0} \right)^2 \right] & \text{for } \varepsilon \leq \varepsilon_0 \\ f_c \left( 1 - 0.15 \frac{\varepsilon - \varepsilon_0}{\varepsilon_{cu} - \varepsilon_0} \right) & \text{for } \varepsilon > \varepsilon_0 \end{cases} \quad (1)$$

$$\sigma_t = \begin{cases} E \times \varepsilon & \text{for } \varepsilon \leq \varepsilon_{cr} \\ f_t & \text{for } \varepsilon_{cr} < \varepsilon \leq \varepsilon_0 \\ \left( \frac{2\varepsilon_{cr}}{\varepsilon} \right)^{0.4} & \text{for } 2\varepsilon_{cr} < \varepsilon \end{cases} \quad (2)$$

$$\varepsilon_0 = 1.8(f_c/E) \quad (3)$$

where  $f$  and  $\sigma$  is the strength and stress with subscripts of  $c$  and  $t$  implying the compression and tension,  $\varepsilon_{cu}$  is the crushing strain of 0.0038,  $\varepsilon_0$  is the strain at  $f_c$  which is expressed by Eq. 3, and  $\varepsilon_{cr}$  is the cracking strain, respectively.

The material properties of the concrete are listed in Table 1, including parameters of density ( $\rho$ ), elastic modulus ( $E$ ), Poisson's ratio ( $\nu$ ), dilation angle ( $\psi$ ), eccentricity ( $m$ ), the ratio of biaxial to uniaxial compressive strength ( $\beta$ ) and invariant ratio ( $K_c$ ).

Table 1. Material properties of the concrete [4]

$\rho$ (ton/mm <sup>3</sup> )	$E$ (GPa)	$\nu$	$f_c$ (MPa)
$2.2 \times 10^{-9}$	28	0.18	48.54
$\psi$	$m$	$\beta$	$K_c$
34	0.1	1.16	0.667

An elastic-plastic model with isotropic hardening was considered to represent the behaviors of steel components, such as liner, rebar, and tendon, which can be represented by Eq. 4 [3]. The material properties of steel components are shown in Table 2. In particular,  $\nu$  is 0.3 for all the steel components.

$$f = \sigma_e - \sigma_y = \left( \frac{3}{2} s : s \right)^{1/2} - \sigma_y \quad (4)$$

where  $s$  is the deviatoric stress,  $\sigma_e$  is the von Mises stress, and  $\sigma_y$  is the yield stress.

Table 2. Material properties of steel components [4]

Component	$\rho$ (ton/mm <sup>3</sup> )	$E$ (GPa)	$\sigma_c$ (MPa)
Rebar	$7.85 \times 10^{-9}$	185	440.4
Liner	$7.80 \times 10^{-9}$	200	376.2
Tendon	$7.41 \times 10^{-9}$	200	1,592.7

## 2.2 Details of FE Model

As shown in Fig. 1, the major components, including concrete structure, liner, rebar and tendon of the 1/4-scaled PCCV were modeled in three dimensions using the guideline suggested by Hesseimer and Dameron [8]. Details of the FE modeling can be found in Cho et al. [6]. For the FE modeling, 3D, 8-node (C3D8) for concrete, 3D, 4-node (M3D4) for liner, and 3D, 2-node (T3D2) for rebar were selected for structural analysis.

As shown in Fig. 2(a), an internal pressure of up to 3.3  $P_d$  ( $P_d = 0.39$  MPa) was applied perpendicular to the surface of the liner. As depicted in Fig. 2(b), all degrees of freedom, including node and element, are constrained at the bottom of the basemat [3].

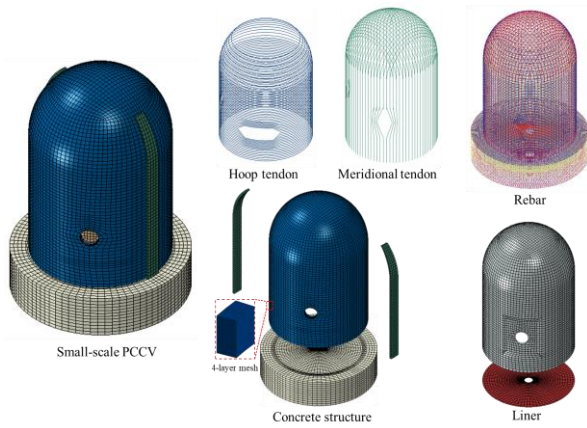


Fig. 1. Finite element model of 1/4-scaled PCCV [3]

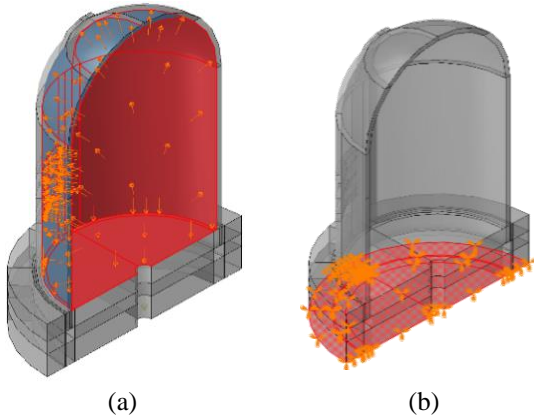


Fig. 2. Schemes of (a) pressure loading conditions and (b) boundary conditions [3]

As seen in Fig. 3, measured radial displacements at four different elevations [1] were compared with FE analysis results of the developed FE model with the same azimuth of 135° [3] to confirm the reliability of the 300 mm element size FE model. Although the analysis result at 10,750 mm shows little variance with a maximum disagreement of roughly 6.9% at 1.29 MPa (3.3  $P_d$ ) [3], the numerical results at three elevations (4,680, 6,200, and 7,730 mm) are generally consistent with those derived from the test data.

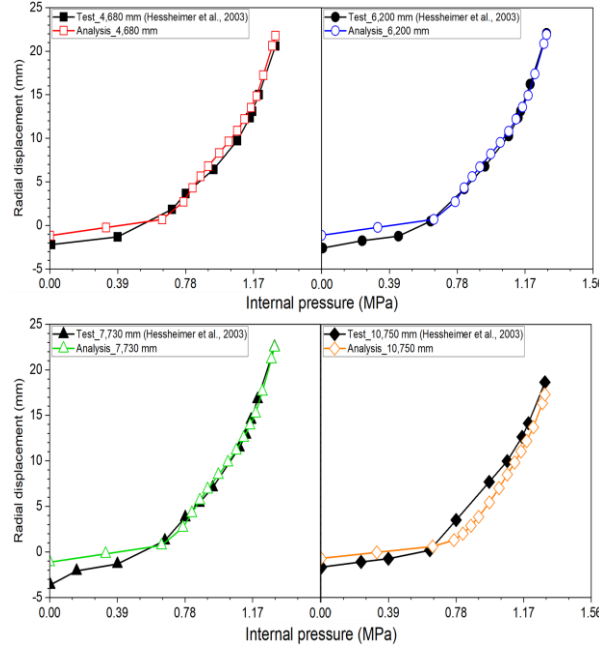


Fig. 3. Comparison of radial displacements between test data and numerical results [3]

## 3. Internal Pressure Capacity at Liner Failure of the PCCV under the Hydrogen Burning Conditions

The hydrogen burning condition was introduced by the MELCOR code for the 4-loop PWR type, similar to the Ohi-3 [9]. In this scenario, the normal operating pressure and temperature were set for the initial conditions, leading to the failure of the hot leg nozzle, hydrogen burn, core meltdown, and failure of the reactor pressure vessel due to the trip of the coolant pump [9]. The temperature and pressure histories at hydrogen burning conditions are shown in Fig. 4.

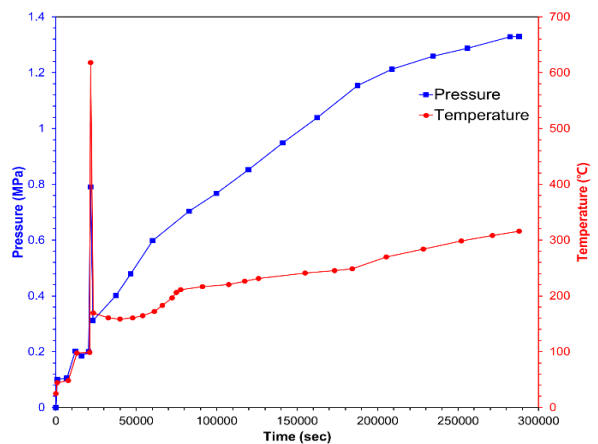


Fig. 4. Temperature and pressure histories under hydrogen burning conditions [9]

### 3.1 Thermal Behavior of the PCCV under Hydrogen Burning Conditions

For the heat transfer analysis, the element types were changed to linear heat transfer brick (DC3D8) for concrete, 4-node heat transfer quadrilateral shell (DS4) for liner, and 2-node heat transfer link (DC1D2) for rebar and tendon [4]. Also, the thermal properties of each component were considered, as shown in Table 3.

Table 3. Thermal properties for concrete and steel [4,9]

Component	Conductivity (W/m×°C)	Specific heat (J/kg×°C)	Thermal expansion (°C <sup>-1</sup> )
Concrete	1.4	879	$1.0 \times 10^{-5}$
Steel	45	470	$1.2 \times 10^{-5}$

Variations in mechanical properties according to temperature were regarded for concrete and steel, as illustrated in Eqs. 5 to 8 [4,9].

$$\text{Concrete strength ratio } S_{Rc} = \exp^{- (T/632)^{1.8}} \quad (5)$$

$$\text{Concrete modulus ratio } M_{Rc} = (S_{Rc})^{0.5} \quad (6)$$

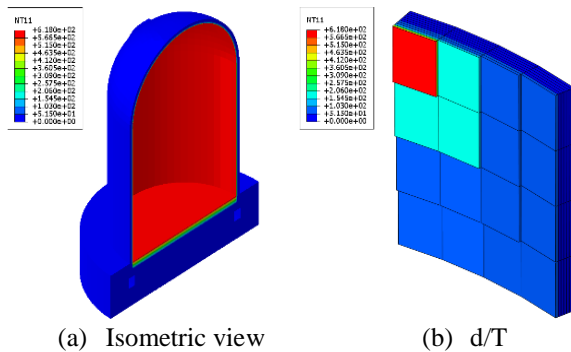
$$\text{Steel yield strength ratio } \begin{aligned} S_{Rs} &= \exp^{- ((T - 340)/300)^{1.9}} \\ S_{Rs} &= 1.0, T \leq 340^\circ\text{C} \end{aligned} \quad (7)$$

$$\text{Steel modulus ratio } M_{Rs} = S_{Rs} \quad (8)$$

In order to conduct the heat transfer analysis, the thermal boundary conditions were imposed at the outer surface of the concrete region of the PCCV, involving free convection with air at a sink temperature of 25 °C [4]. Also, the heat conduction from the basemat into soil, with the same sink temperature of 25 °C, was considered. Equations 9 and 10 describe heat transfer coefficients varying with temperature [4,9].

$$h_{\text{conv}} = 4.80(\Delta T)^{1/3} \text{ W/m}^2 \cdot \text{K} \quad (9)$$

$$h_{\text{cond}} = 0.0724 \text{ W/m}^2 \cdot \text{K} \quad (10)$$



(a) Isometric view (b) d/T  
Fig. 5. Temperature distribution at the hydrogen burning condition (unit: °C) [4]

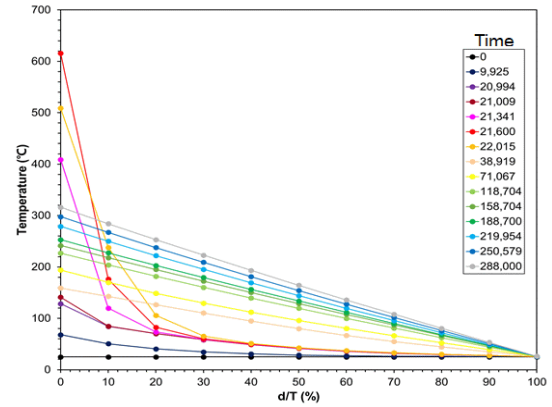


Fig. 6. Temperature gradients of concrete according to time [4]

The temperature input suggested in Fig. 4 was applied on the nodes of the liner for the heat transfer analysis [4]. Figure 5 depicts the temperature distribution at the hydrogen burning conditions with the peak temperature of 618 °C, where d/T implies the depth per thickness [4]. Figure 6 shows the temperature gradients of the concrete along the thickness direction according to time [4].

### 3.2 Mechanical Behavior of the PCCV under Hydrogen Burning Conditions

Structural analysis was conducted to evaluate the mechanical behavior and performance of the PCCV loaded by temperature and internal pressure loads [4]. Through the \*Predefined Field, temperature option provided by the ABAQUS, the heat transfer analysis result was imposed as thermal boundary conditions [4]. For this study, only functional failure by the liner tearing was studied using the failure criterion of 0.3 % of the liner strain suggested by ASME Section III, Division 2, sub-article CC-3720 [10].

Figures 7(a) and 7(b) show the distribution of liner strain near the equipment hatch (EH) region, where the maximum strain was developed, and the free field (FF) region away from discontinuities, respectively [4]. At the termination time (288,000 sec), the maximum strain of 2.36 % occurred at the right edge of the EH and the strain at the FF was 1.51%, respectively [4].

Figure 8 describes the maximum principal strains of the liner at the EH and FF compared with the failure criterion of 0.3% of the liner strain [4]. At the EH, the liner tearing is expected to occur at 0.79 MPa at point A and 0.57 MPa at point B, respectively [4]. At the FF, the liner tearing is expected to occur at the 0.79 MPa at point A and 0.61 MPa at point B, respectively [4]. Compared to the internal pressure capacity of 1.29 MPa of the PCCV without thermal load, the failure was predicted to be 0.50 MPa lower at point A [4]. At point B, decrease in internal pressure capacity was 0.72 MPa at the EH and 0.68 MPa at the FF, respectively [4]. The internal pressure capacity of the PCCV decreased by 56 % at the EH and 53 % at the FF, respectively [4].

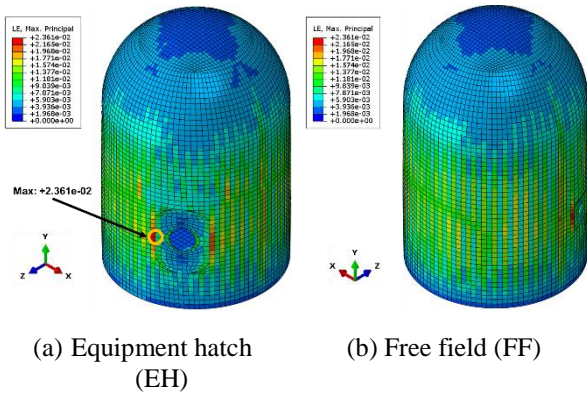


Fig. 7. Distributions of maximum principal strain of the liner (unit: mm/mm) [4]

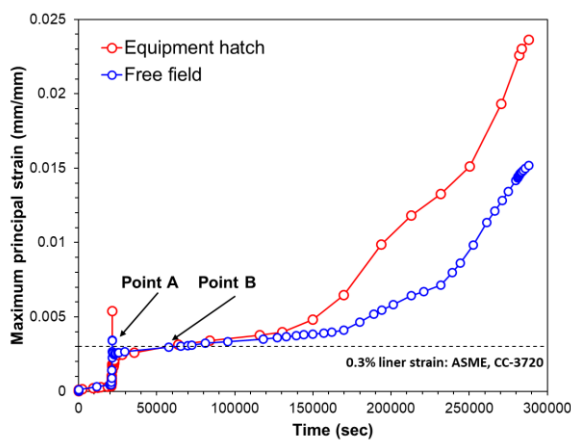


Fig. 8. Maximum principal strains of liner at the EH and FF regions [4]

#### 4. Conclusion

The objective of this study was to assess the internal pressure capacities of the PCCV in the event of liner failure, while considering the combined effects of temperature and internal pressure under hydrogen burning conditions. Findings are highlighted below.

- (1) The accuracy of the finite element model for the PCCV was validated through a comparative study.
- (2) Heat transfer analysis was performed, by considering not only the degradations in the material properties according to temperature but also heat transfer coefficients for the convection and conduction, and its result was mapped at the structural analysis.
- (3) The failure pressures were investigated using the ASME criterion of 0.3% liner's strain. At the peak (21,600 sec) of the temperature and internal pressure caused by the hydrogen burn, both of EH and FF were expected to lose their integrity.
- (4) When thermal loads were taken into account, the internal pressure capacity of the PCCV decreased by 56% at the EH and 53% at the FF.

#### ACKNOWLEDGMENT

This work was supported by the Nuclear Safety Research Program through the Korea Foundation of Nuclear Safety (KoFONS) using the financial resource granted by the Nuclear Safety and Security Commission (NSSC) of the Republic of Korea (No. 2106008).

#### REFERENCES

- [1] Hessheimer, M.F., Klamerus, E.W., Lambert, L.D., Rightley, G.S., Dameron, R.A. 2003. Overpressurization test of a 1:4-scale prestressed concrete containment vessel model. Technical Report No. NUREG/CR-6810, SAND2003-0840P, U.S. Nuclear Regulatory Commission, Washington, DC, USA.
- [2] Nguyen, D., Thusa, B., Park, H.S., Azad, M.S., Lee, T.H. 2021. Efficiency of various structural modeling schemes on evaluating seismic performance and fragility of APR 1400 containment building. Nuclear Engineering Technology, 53(8), 2696-2707.
- [3] Cho, W.M., Ha, S.K., Kang, S.H.S., Chang, Y.S. 2023. A numerical approach for assessing internal pressure capacity at liner failure in the expanded free-field of the prestressed concrete containment vessel, Nuclear Engineering Technology 55, 3677-3691.
- [4] Woo, H.S., Cho, W.M., Ha, S.K., Chang, Y.S. 2024. Numerical study on the fragility of the small-scaled prestressed concrete containment vessel under severe accident conditions, In preparation.
- [5] ABAQUS-6.12. 2018. ABAQUS analysis user's manual. ABAQUS 6.12, Dassault Systèmes Simulia Corp., Providence, RI, USA.
- [6] Hognestad, E. 1951. A study on combined bending and axial load in reinforced concrete members. University of Illinois at Urbana-Champaign, IL, 43-46. Bulletin.
- [7] Izumo, J., Shima, H., Okamura, H., 1989. Analytical model for RC panel elements subjected to in-plane forces. Concrete Library Japan Society of Civil Engineers. 12, 155-181.
- [8] Hessheimer, M.F., Dameron, R.A., 2006. Containment integrity research at Sandia national laboratories-an overview. Technical Report No. NUREG/CR-6906, SAND2006-2274P, U.S. Nuclear Regulatory Commission, Washington, DC, USA.
- [9] Jovall, O., Paalsson, M., Svaerd, B., Larsson, Jan-Anders. 2005. ISP 48: Posttest analysis of the NUPEC/NRC 1:4-scale prestressed concrete containment vessel model (NEA-CSNI-R-2005-05), Nuclear Energy Agency of the OECD (NEA).
- [10] ASME Boiler and Pressure Vessel Code, Section III, 2021. Rules for Construction of Nuclear Power Plant Components, Division 2, American Society of Mechanical Engineers, New York, NY.